Linking solar bosonic dark matter halos and active neutrinos

Ilídio Lopes[*]

Centro de Astrofísica e Gravitação—CENTRA, Departamento de Física, Instituto Superior Técnico—IST, Universidade de Lisboa—UL, Avenida Rovisco Pais 1, 1049-001 Lisboa, Portugal

(Received 21 July 2022; accepted 1 September 2023; published 20 October 2023)

Our study investigates the complex interaction between active neutrinos and the ultralight bosonic dark matter halo surrounding the Sun. This halo extends over several solar radii due to the Sun's gravitational field, and we represent it as a coherent oscillating classical field configuration of bosonic dark matter particles that vary in time. Our investigation has revealed that, based on the available solar neutrino flux data, these novel models do not surpass the performance of the conventional neutrino flavour oscillation model. Furthermore, we discuss how next-generation solar neutrino detectors have the potential to provide evidence for the existence or absence of the ultralight-dark matter halo.

DOI: 10.1103/PhysRevD.108.083028

I. INTRODUCTION

While studying the movement of galaxies in the Coma cluster, Fritz Zwicky became the first astronomer to detect a discrepancy between visible matter and gravitational forces. In a groundbreaking 1933 article, he presented a compelling finding: the visible matter's total mass in the cluster was insufficient to gravitationally bind the galaxies, identifying what is now known as the dark matter problem [1]. Since then, many solutions have continuously been put forward to solve this problem, including invisible massive astronomical bodies such as black holes, alternative theories to general gravity, extensions to the standard model of fundamental particles and interactions postulating the existence of new particles. Although many articles are being published on these very active research fields, the latter class of solutions is the most popular and widely accepted. However, identifying the definitive new particle or particles remains a significant challenge [2]. So far, the theoretical and experimental efforts to discover such particles have focused primarily on the so-called weakly interacting massive particles (WIMPs). Accordingly, these particles are neutral and nonrelativistic particles, with masses varying from a few GeV to 10^3 GeV and interacting ultraweakly with the standard particles, e.g., [3,4].

The lack of evidence for the existence of WIMPs and the need to answer unsettled problems in the current standard cosmological model—Lambda cold dark matter model—motivated the study of properties of ultralight particles as viable dark matter candidates. These particles are well motivated by modern theories (e.g., [5]), many of which predict the existence of spin-0 and spin-1 bosons, including axions or axionlike particles and dark photons [5–7]. These ultralight particles collectively behave like a bosonic field. In this work, we call all these particles, including the classical axion [8] or their closest relative, the axionlike particles [9], simply "bosons" or "ultralight particles" if not stated otherwise. Interestingly, we should be able to detect such fields by their interaction with standard particles in the future. A cornucopia of experiments aims to detect such bosonic particles by the emission of photons created by their interaction with magnetic fields [10], nuclear magnetic resonance (e.g., [11]) and axion spin precession (e.g., [12]).

Here, we discuss the possibility of this ultralight-dark matter particle interacting with solar neutrinos using a well-established model for predicting neutrino flavor oscillation through vacuum and matter. In this work, we discuss also how current and future solar neutrino detectors (e.g., [13]) could be used to constrain the properties of these particles.

The article is organized as follows: Sec. II presents the properties of the local dark matter field. Section III explains the mechanism by which the local dark matter field interacts with the active neutrinos. Section IV introduces the survival probability of electron neutrino function in the standard neutrino oscillation flavor model. Section V generalizes the result of the previous section to the new neutrino dark matter model. Section VI discusses the time dependence of the survival probability of electron neutrinos. Section VII gives predictions of the new neutrino model for the present Sun, and Sec. VIII summarizes the main results and conclusions of this work.

If not stated otherwise, we work in natural units ($c = \hbar = 1$). All standard units are expressed in GeV by applying the usual conversion rules. These are the most common ones used in this work: $1\ \mathrm{m} = 5.068 \times 10^{15}\ \mathrm{GeV}^{-1}$, $1\ \mathrm{kg} = 5.610 \times 10^{26}\ \mathrm{GeV}$, and $1\ \mathrm{sec} = 1.519 \times 10^{24}\ \mathrm{GeV}^{-1}$.

[*]ilidio.lopes@tecnico.ulisboa.pt

II. ULTRALIGHT-DARK MATTER

A. The origin of the ultralight-dark matter field

If boson particles exist today, they were produced abundantly in the early Universe. The production of light-dark matter can take many forms. We have thermal production, dark matter decay, parametric resonance, and topological defect decay, among other mechanisms (e.g., [14,15]). For the light-dark matter field, some authors obtained $\Omega_\psi^2 = 0.1(a_o/10^{17}\ \mathrm{GeV})^2 \quad (m_\psi/10^{-22}\ \mathrm{eV})^{1/2}$, where a_o is a parameter that relates to the initial misalignment angle of the axion, and m_ψ is the axion mass [16,17]. Therefore, we will assume that at least a fraction of the dark matter *background* in the solar neighborhood is made of an ensemble of ultralight bosons,

$$\bar{\rho}_{b\psi} = \bar{\rho}_{\mathrm{DM}}^{\odot}\left(\frac{\Omega_\psi h^2}{\Omega_{\mathrm{DM}} h^2}\right), \tag{1}$$

where $\bar{\rho}_{\mathrm{DM}}^{\odot}$ is the local density of dark matter (DM) in the solar neighborhood, $\Omega_{\mathrm{DM}}^2 h^2$ and $\Omega_\psi^2 h^2$ are the total DM and axion energy density parameters in the present Universe, and h is the reduced Hubble constant such that $h \equiv H_0/(100\ \mathrm{km\,s^{-1}\,Mpc^{-1}})$. Recent measurements of the dark matter constituents give $\rho_{\mathrm{DM}}^{\odot} = 0.39\ \mathrm{GeV\,cm^{-3}}$ [18] and $\Omega_{\mathrm{DM}} h^2 = 0.12$ [19]. Now, we compute the averaged density number of dark matter $\bar{n}_{b\psi}$ near the Sun as the ratio between the averaged local density $\bar{\rho}_{b\psi}$ and m_ψ, such that $\bar{n}_{b\psi} = \bar{\rho}_{b\psi}/m_\psi$. For example, considering axions with $m_\psi = 10^{-22}\ \mathrm{eV}$ and $\Omega_\psi h^2 = \Omega_{\mathrm{DM}} h^2$, we obtain $\bar{n}_{b\psi} = 3.9 \times 10^{30}\ \mathrm{cm^{-3}}$. This value is only 2 orders of magnitude smaller than the density of electrons in the Sun's core, $\bar{n}_e \sim 6 \times 10^{31}\ \mathrm{cm^{-3}}$ [20].

Ultralight boson particles behave as nonrelativistic matter and account for dark matter in the present Universe. Moreover, such a population of particles will smooth inhomogeneities in the dark matter distribution on scales smaller than the de Broglie wavelength λ_{dB}. We have calculated the de Broglie wavelength, which is given by the equation $\lambda_{\mathrm{dB}} = 1.24 \times 10^{22}\ (10^{-23}\ \mathrm{eV}/m_\psi)\ (10^{-3}/v_\psi)\ \mathrm{cm}$, where v_ψ is the virial velocity of the boson in the halo. For the fiducial boson, assuming $m_\psi = 1.5 \times 10^{-14}\ \mathrm{eV}$ and $v_\psi \sim 10^{-3}$, we obtain $\lambda_{\mathrm{dB}} = 119 R_\odot$. Collectively, such particles form a dark matter background that we choose to represent as a coherent oscillating classical field configuration (e.g., [21–23]). Accordingly, the general form of this field reads

$$\psi_b(\vec{r}, t) = \psi_{bo}\ \cos(m_\psi t + \epsilon_o), \tag{2}$$

where ψ_{bo} and ϵ_o are the amplitude and phase of this bosonic field background. The amplitude ψ_{bo} is computed from the density $\bar{\rho}_{b\psi}$ as $\psi_{bo} = \sqrt{2\bar{\rho}_{b\psi}}/m_\psi$ and we assume that $\epsilon_o \approx 0$ [22]. In the determination of $\psi_b(\vec{r}, t)$, since $v_\psi \sim 10^{-3}$ is very small (e.g., [23]), we neglect its contribution for Eq. (2).

Here, we hypothesize that ultralight bosons around the Sun form a halo of dark matter. As a consequence of such a gravitational bound system, we describe the boson field of this bound system similar to Eq. (2). Conveniently, we define $\bar{\rho}_\psi$ as the average dark matter density inside the halo. Since $\bar{\rho}_\psi$ is larger than background density $\bar{\rho}_{b\psi}$, we have $\bar{\rho}_\psi = \chi_\psi \bar{\rho}_{b\psi}$, where χ_ψ is a positive number larger than 1. The boson halo we are considering shares similar properties to boson stars (e.g., [24,25]), except that it is bounded by a gravitational potential of the host star, the Sun, rather than its self-gravity. Since these particles in the halo are maintained and stabilized by the gravitational potential of the host star, the total mass of halo M_ψ must be much smaller than the mass of the star $M_\odot$, i.e., $M_\psi < M_\odot$, so specifically we can consider that $M_\psi \leq M_\odot/2$.

B. The local ultralight-dark matter field

Our study focuses on a halo of ultralight bosons hosted by the Sun, which we assume to be a spherical object with a total radius R_ψ large enough to encompass the entire Sun. For convenience, we use a fiducial radius several times greater than the Sun's. In the nonrelativistic limit, we compute the boson field inside of the halo similar to boson stars as originally proposed by Kaup [26] and Ruffini and Bonazzola [27], following in the footsteps of Wheeler [28]. A recent review of the properties of boson stars can be found in Braaten and Zhang [29]. Within the nonrelativist effective field theory framework, Namjoo *et al.* [30] derived an exact connection between the boson field, a real function, and a complex function known in this context as a relaxation wave function. Chavanis [31] found that an exponential form is a suitable ansatz for describing the radial variation of the density profile inside the halo. Eby *et al.* [32] has shown this form to be a good fit for the numerical solution to the Gross-Pitaevskii-Poisson equation [33]. In our case, we consider that the boson field decays exponentially with the distance r from the star's center [31]. Therefore, the boson field created by the halo of dark matter particles in the presence of an external gravitational source reads

$$\psi(r, t) = \sqrt{\frac{M_\psi}{\pi m_\psi R_\psi^3}} e^{-\frac{r}{R_\psi}} \cos(m_\psi t). \tag{3}$$

In this configuration, the radius of a halo R_ψ is determined by the gravitational potential of the external source: $R_\psi = (M_p^2/M_\odot) m_\psi^{-2}$, where $M_p = (\hbar c/G)^{1/2} = 1.2 \times 10^{19}\ \mathrm{GeV}$ is the Planck mass, or $R_\psi = 3.7863(1 \times 10^{-13}\ \mathrm{eV}/m_\psi)^2\ R_\odot$. Our study will focus on dark matter halos with a radius of at least 2 times that of the solar radius ($R_\psi \geq 2R_\odot$), which implies the presence of dark matter particles with a mass

m_ψ lower than the critical threshold of $m_\psi^c \approx 3.6 \times 10^{-13}$ eV. The boson field $\psi(\vec{r}, t)$ [Eq. (3)] inside the halo behaves similar to the boson background field $\psi_b(\vec{r}, t)$ [Eq. (2)]. Both fields are oscillating in time with a frequency approximately equal to the boson mass m_ψ (e.g., [34]). We also found that the density profile of the dark matter halo (for $r \leq R_\psi$ with $R_\psi \geq R_\odot$) reads

$$\rho_\psi(r) = \rho_{c\psi} e^{-\frac{2r}{R_\psi}}, \tag{4}$$

where $\rho_{c\psi} = M_\psi/(\pi R_\psi^3)$. This expression is identical to the one found by Banerjee *et al.* [35] for relaxion stars.

We compute the overdensity of particles inside the halo in a similar way to the calculation done for the boson star [35]: the averaged density $\bar{\rho}_\psi$ of the halo is determined in comparison to the background density of the dark matter $\bar{\rho}_{b\phi}$, in such a way that the parameter of condensation χ_ψ corresponds to

$$\chi_\psi = \frac{\bar{\rho}_\psi}{\bar{\rho}_{b\psi}} \approx \frac{M_\psi}{\pi R_\psi^3} \frac{1}{\bar{\rho}_{b\psi}}. \tag{5}$$

If we set $\bar{\rho}_{b\phi} = \bar{\rho}_{\rm DM}^\odot$ and express M_ψ in units of solar masses, the previous equation can be rewritten as follows:

$$\chi_\psi = 4.987 \times 10^{22} \left(\frac{M_\psi}{M_\odot}\right) \left(\frac{m_\psi}{1 \times 10^{-13}\ \text{eV}}\right)^6, \tag{6}$$

where m_ψ does not exceed the critical threshold value of m_ψ^c.

The standard solar model, which is based on solar neutrino fluxes and helioseismology data, provides an accurate understanding of the physics within the Sun (e.g., [36]). Based on this, we assume that the total mass of the halo must be sufficiently light to have a negligible effect on solar gravity and structure. Furthermore, Banerjee *et al.* [35] found that planetary ephemerides data can exclude dark matter halos with a total mass greater than $10^{-12} M_\odot$. As a result, we have adopted a total mass of $10^{-13} M_\odot$ for our dark matter halo unless otherwise specified. Our fiducial model assumes $m_\psi = 1.5 \times 10^{-14}$ eV and $M_\psi = 10^{-13} M_\odot$, which yields $R_\psi = 168 R_\odot = 0.783$ A.U.. and $\chi_\psi = 5.69 \times 10^4$. Occasionally, we consider a larger mass for the dark matter halo, such as $M_\psi = 10^{-10} M_\odot$.

III. ACTIVE NEUTRINOS PROPAGATING IN A BOSON DARK MATTER FIELD

Here, we choose to explore the physics beyond the standard model by encoding nonstandard interactions between active neutrinos and dark matter [37] in the framework of effective field theory (e.g., [38]). We start by considering an extended version of the standard neutrino flavor oscillations model [39], which includes an additional nonstandard interaction: we postulated that the three active neutrinos ν_a ($a = e, \tau, \mu$) could change their flavor through an interaction with an ultralight time-dependent boson field $\psi(r, t)$ [Eq. (3)], mediated by vector boson ϕ with a mass m_ϕ. Therefore, ψ couples with ν_a by the interaction $g_\psi \psi \nu_a \nu_a$, where g_ψ is a dimensionless coupling (e.g., [40]). Moreover, to widen the space of possible solutions, the intermediate boson ϕ can be an ultralight particle. Accordingly, the effective Lagrangian (e.g., [41]) that describes the system is

$$\mathcal{L} \supset -m_\nu \left(1 + g_\psi \frac{\psi}{\Lambda}\right) \nu\nu + \text{H.c.}, \tag{7}$$

where $\Lambda = m_\nu/g_\psi$ is a large mass scale (for instance, with a $g_\psi \ll 1$). For convenience, we suppress the flavor indices on ν and m_ν. The results found in this work are equally valid for Dirac and Majorana neutrinos. Therefore, the survival probabilities of solar neutrinos can vary through two new mechanisms:

(1) Neutrino masses inside the dark matter halo can change according to Eq. (7): m_ν can vary to $m_\nu(1 + \delta m_\nu/m_\nu)$ by the action of the boson field. Here we consider a large number of bosons within the de Broglie wavelength, making them oscillate coherently as a single classical field, such as $\psi(r, t)$ corresponds to the boson field defined in Eq. (3), for which the mass perturbation reads

$$\frac{\delta m_\nu}{m_\nu} = \bar{\epsilon}_\psi e^{-\frac{r}{R_\psi}} \cos(m_\psi t), \tag{8}$$

where the amplitude $\bar{\epsilon}_\psi$ reads

$$\bar{\epsilon}_\psi = \frac{\sqrt{m_\psi}}{2} \frac{g_\psi \sqrt{2\chi_\psi \bar{\rho}_{\rm DM}^\odot}}{m_\nu m_\psi} \left(\frac{h^2 \Omega_\psi}{h^2 \Omega_{\rm DM}}\right)^{1/2}. \tag{9}$$

If not stated otherwise, we assume that $\Omega_\psi h^2 = \Omega_{\rm DM} h^2$. Note that $\bar{\epsilon}_\psi$ can affect neutrino flavors' transformation even if $\Omega_\psi h^2$ is a small fraction of the dark matter halo. Lopes ([42] and references therein) discusses the properties of such a dark matter model.

(2) The forward scattering of active neutrinos ν_a can change due to the boson field ψ and the intermediator vector boson ϕ.[1] Such effect is taken into account by the inclusion of a new term $V_{\psi\nu_a}$ in the matter

[1]We note that the MSW potential resulting from the interaction of neutrinos with a boson field through a fermionic mediator is identical to the interaction of neutrinos with a fermion field through a bosonic mediator [43]. The two particles switch roles in the MSW potentials. The difference between the two MSW potentials may only appear in higher-order terms.

potential diagonal matrix $\mathcal{V}$ (e.g., [44]). The function $V_{\psi\nu_a}$ is an effective Wolfenstein potential of ψ particles associated with flavor change due to the propagation of neutrinos inside the dark matter limit medium. Such neutrino flavor oscillation results from the neutrinos' interaction with bosons ψ through ϕ. This process corresponds to the well-known Mikheyev-Smirnov-Wolfenstein effect (MSW) [45,46]. The $V_{\psi\nu_a}$ inside the boson halo for a generic mediator ϕ [40] reads

$$V_{\psi\nu_a}(r) = g_\psi g_{\nu_a} \begin{cases} \bar{V}^{\mathrm{I}}_\psi(r) + \bar{V}^{\mathrm{II}}_\psi(r), & r \le R_\psi, \\ \bar{V}^{\mathrm{III}}_\psi(r), & r \ge R_\psi, \end{cases} \tag{10}$$

where g_ψ and g_{ν_a} represent the coupling constants of the corresponding particle—boson and active neutrino, associated with an intermediator particle with mass m_ϕ [37]. The radial functions $\bar{V}^{\mathrm{I}}_\psi(r)$, $\bar{V}^{\mathrm{II}}_\psi(r)$, and $\bar{V}^{\mathrm{III}}_\psi(r)$ are given by the following expressions:

$$\bar{V}^{\mathrm{I}}_\psi(r) = \frac{e^{-m_\phi r}}{m_\phi r} \int_0^r r' \bar{n}_\psi(r') \sinh\,(m_\phi r') dr', \tag{11}$$

$$\bar{V}^{\mathrm{II}}_\psi(r) = \frac{\sinh\,(m_\phi r)}{m_\phi r} \int_r^{R_\psi} r' \bar{n}_\psi(r') e^{-m_\phi r'} dr', \tag{12}$$

and

$$\bar{V}^{\mathrm{III}}_\psi(r) = \frac{e^{-m_\phi r}}{m_\phi r} \int_0^{R_\psi} r' \bar{n}_\psi(r') \sinh\,(m_\phi r') dr', \tag{13}$$

where $n_\psi(r)$ is the local density of bosons given by

$$n_\psi(r) = \frac{\rho_\psi(r)}{m_\psi} = \frac{\rho_{c\psi}}{m_\psi} e^{-\frac{2r}{R_\psi}}, \tag{14}$$

where $\rho_\psi(r)$ is given by Eq. (4).

It follows that the Wolfenstein potential $V_{\psi\nu_a}$ [Eq. (10)] now reads

$$V_{\psi\nu_a}(r) = \frac{g_\psi g_{\nu_a} R_\psi^2}{m_\phi^2 R_\psi^2 - 4} n_\psi(r)\,[1 + \Psi(r)]. \tag{15}$$

The coupling g_{ν_a} is different for neutrinos with different flavors: ν_a ($a = e,\ \nu,\ \tau$). The function $\Psi(r)$ is given by

$$\Psi(r) = \frac{4}{m_\phi^2 R_\psi^2 - 4} \frac{R_\psi}{r} [e^{-(m_\phi R_\psi - 2)\frac{r}{R_\psi}} - 1]. \tag{16}$$

This result corresponds to the effective potential of spherically symmetric exponential density distribution [40]. If R_ψ is much larger, then the effective potential corresponds to a pointlike interaction: $V_{\psi\nu_a} = g_\psi g_{\nu_a} n_\psi / m_\phi^2$. We remind the reader that ν can be one of the following flavors: ν_e, ν_τ, or ν_μ.

We remind the reader that the interaction between dark matter particles with neutrinos and antineutrinos depends intrinsically on the nature of the dark matter particle and the particle mediator. In this work, without loss of generality, we assume that the dark matter interacts with neutrinos but not with antineutrinos. It is worth reminding the reader that such asymmetry is already present in the standard MSW effect (e.g., [45]), since most of the neutrino propagation medium is composed of matter and not antimatter. Moreover, we also include in our calculation the corrections resulting from the propagation (at finite temperature) of neutrinos in a thermal background of dark matter particles (e.g., [47,48]). Several mechanisms contribute to the enhancement or suppression of the conversation of neutrinos from one flavor to another; however, some of these processes are more relevant than others for the neutrino energy window of this study. Here, following Lunardini and Smirnov [49], we include this effect using the effective propagator[2] of the intermediator ϕ defined as $\zeta_\phi = (1 + s_\phi)/[(1 + s_\phi)^2 + \gamma_\phi^2]$, where $s_\phi = 2Em_\psi/m_\phi^2$, $\gamma_\phi = \Gamma_\phi/m_\phi$, and Γ_ϕ is the width of the intermediator particle ϕ. Konstandin and Ohlsson [50] have computed the propagator function using the thermal field theory [51] and found that the propagator function should read $\zeta_\phi = (1 + s_\phi)/[(1 + s_\phi)^2 + s_\phi^2\gamma_\phi^2]$. This last ζ_ϕ expression differs from the expression found by Lunardini and Smirnov [49], only by a term of small magnitude in the dominator of function ζ_ϕ, where $s_\phi^2\gamma_\phi^2$ replaces γ_ϕ^2. Since γ_ϕ is a minimal quantity, both expressions agree with current experiments' data [49]. Therefore, here, we opt for the following expression:

$$\zeta_\phi \equiv \frac{(1 + s_\phi)}{(1 + s_\phi)^2 + \gamma_\phi^2}. \tag{17}$$

It is worth noticing that, in the limit of $s_\phi \gg 1$, we obtain $\zeta_\phi \approx s_\phi^{-1} = m_\phi^2/(2Em_\psi)$. We include the correction on $V_{\psi\nu_a}$ [Eq. (15)], through the function ζ_ϕ [Eq. (17)], hence the Wolfenstein potential now reads

$$V_{\psi\nu_a}(r) = \frac{g_\psi g_{\nu_a} R_\psi^2}{m_\phi^2 R_\psi^2 - 4} n_\psi(r)\,\zeta_\phi\,[1 + \Psi(r)]. \tag{18}$$

We interpret the function ζ_ϕ in $V_{\psi\nu_a}(r)$ as the correction coming from the propagation of neutrinos within an

[2]We note that, for convenience, the definition of the propagator function in this work differs from the one found in the literature [49,50], where $\zeta_o(s_\phi) = (1 - s_\phi)/[(1 - s_\phi)^2 + \gamma_\phi^2]$, therefore $\zeta_\phi = \zeta_o(-s_\phi)$.

effective bosonic-neutrino potential that starts by considering the effect of neutrino propagation on a limited bosonic medium.

IV. SURVIVAL PROBABILITY OF ELECTRON NEUTRINOS: CLASSICAL MODEL

Here, we compute the survival probability of electron neutrinos $P_{ee}(E)$ of several ultralight-dark matter models and compare them with the data coming from solar neutrino detectors. We compute $P_{ee}(E)$ by using one of the analytical formulas found in the literature (e.g., [52–56]). If not stated otherwise, we consider the neutrino oscillations occurring inside the Sun and in the boson halo to be adiabatic. A detailed discussion about adiabatic and nonadiabatic neutrino flavor oscillations is available by Gonzalez-Garcia and Nir [57] and Fantini *et al.* [58]. In agreement with the current neutrino data in which, at a good approximation, the neutrino flavor oscillations between the three flavors are considered adiabatic [56,59,60], and following the recent review of particle physics on this topic [61,62], specifically the article "Neutrino masses, mixing, and oscillations," the survival probability of electron neutrinos reads

$$P_{ee}(E) \approx \cos^4(\theta_{13}) P_{ee}^{2\nu_e} + \sin^4(\theta_{13}), \tag{19}$$

where $P_{2\nu_e}$ is the survival probability in the two neutrino flavor model (with $\theta_{13} = 0$) given by

$$P_{ee}^{2\nu_e}(E) = \frac{1}{2} + \left(\frac{1}{2} - P_\gamma\right) \cos(2\theta_{12}) \cos(2\theta_m), \tag{20}$$

where P_γ is the jump probability that corrects the adiabatic expression (20) for the nonadiabatic contribution, and $\theta_m = \theta_m(r_s)$ is the matter mixing angle at the point of neutrino production (source) located at a distance r_s from the center of the Sun (e.g., [63,64]). The jump probability P_γ [65] reads

$$P_\gamma = \frac{e^{-\gamma \sin^2\theta_{12}} - e^{-\gamma}}{1 - e^{-\gamma}} P_{\rm H}, \tag{21}$$

where $\gamma = 2\pi h_\gamma \Delta m_{21}^2/2E$, h_γ is the scale height [66] and $P_{\rm H}$ is a regular step function.

The matter mixing angle (Gando *et al.* [67]) is given by

$$\cos(2\theta_m) = \frac{A_m}{\sqrt{A_m^2 + \sin^2(2\theta_{12})}}, \tag{22}$$

where A_m reads

$$A_m = \cos(2\theta_{12}) - V_m/\Delta m_{21}^2. \tag{23}$$

In the standard case [59], it corresponds to $V_m = 2V_{cc}\cos^2(\theta_{13})E$ with $V_{cc} = \sqrt{2}G_F n_e(r)$, where $n_e(r)$ is different from zero ($r \leq R_\odot$) only inside the Sun. In the previous expression, V_{cc} is the Wolfenstein potential. Nevertheless, as we will see in the next section, $V_{cc}(r)$ in this study will be replaced by a new effective potential $V_{\rm eff}(r)$.

The maximum production of neutrinos in the Sun's core occurs in a region between 0.01 and 0.25 solar radius, with neutrino nuclear reactions of the proton-proton chain and carbon-nitrogen-oxygen cycle occurring at different locations (e.g., [20]). These neutrinos, produced at various values of r_s, when traveling toward the Sun's surface, follow paths of different lengths. Moreover, during their traveling, neutrinos experience varying plasma conditions, including rapid decreasing of the electron density from the center toward the surface. In general, we expect that nonadiabatic corrections average out and are negligible along the trajectory of the neutrinos, except at the boundaries (layer of rapid potential transition) of the neutrino path, typically around the neutrino production point or at the surface of the Sun.[3] Therefore, we could expect Eq. (20) to be very different when taking such effects into account. Nevertheless, this is not the case, de Holanda *et al.* [68] analyzed in detail the contribution to P_{ee} (Eq. (19) coming from nonadiabaticity corrections and variation on the locations of neutrino production, i.e., r_s, and they found that the impact is minimal. In general, P_γ [Eq. (21)] is expected to take a real value, such that $P_\gamma = 0$ or $P_\gamma \neq 0$ corresponding to neutrino flavor adiabatic and nonadiabatic conversions. In general, the conversions are only called nonadiabatic if P_γ is non-negligible. Figure 1 depicts the survival probability $P_{ee}(E)$ for the standard neutrino flavor oscillation model. Interestingly, the contribution of P_γ to $P_{ee}(E)$ is minimal, bordering on negligible. In this figure, the red and blue curves represent $P_{ee}(E)$, as defined by Eq. (20), with and without the P_γ contribution, respectively, the latter being determined by Eq. (21).

Since the electron number density n_e varies considerably along the neutrino path in the Sun: n_e decreases monotonically from the 10^{31} m^{-3} in the center of the star to an almost negligible value at the surface, e.g., [20]. Therefore, neutrinos propagating toward the surface necessarily cross a layer of matter where $n_e = n_{\rm res}$ such that $A_m = 0$. This particular solution of the function A_m, the value for which $n_{\rm res}(E)$ leads to $A_m = 0$, is known as the resonance condition. In the classic case, we compute this electronic density associated with the resonance condition as

$$n_e(r) = n_{\rm res}(E) \equiv \frac{\Delta m_{21}^2}{2\sqrt{2}G_F E} \frac{\cos(2\theta_{12})}{\cos^2(\theta_{13})}, \tag{24}$$

where $r = r_\gamma$ ($\neq h_\gamma$) is defined as the layer where the resonance condition $n_e(r) = n_{\rm res}(E)$ occurs. Figure 2 shows $n_{\rm res}(r)$ for the present Sun as a continuous red

[3]Since the potential is zero at the Sun's surface, the nonadiabatic contribution is negligible.

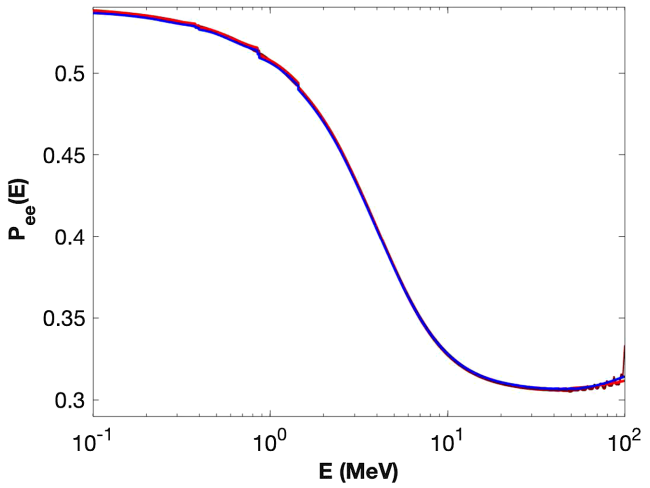

FIG. 1. This figure illustrates the survival probability of the electron neutrino $P_{ee}(E)$ computed for the standard model of neutrino flavor oscillations (model S_ν, as detailed in Table I). The calculations, based on Eqs. (19) and (20), also factor in the jump probability term P_γ [Eq. (21)]. The red curve includes the P_γ contribution, as per Eq. (21), while the blue curve depicts $P_{ee}(E)$ without the P_γ contribution. While the contribution of P_γ to $P_{ee}(E)$ remains negligible within the shown neutrino energy interval, its influence becomes marginally visible for neutrino energies exceeding 50 MeV. For more details, please refer to the main text.

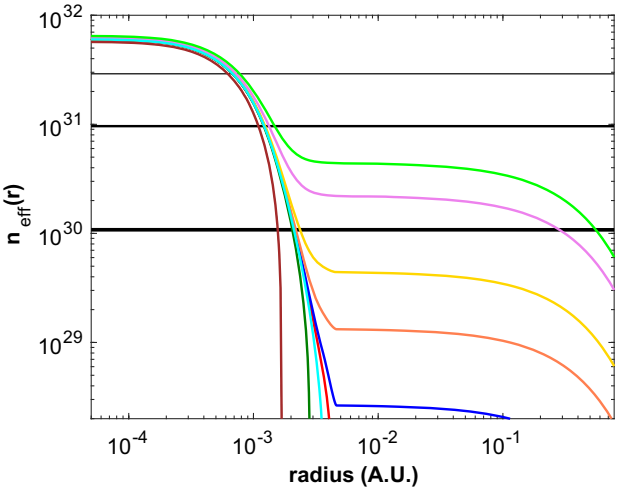

FIG. 2. The effective density $n_{\rm eff}(r)$ is shown as a function of radius within a spherical boson halo with a radius of $R_\psi = 0.783$ A.U. and a total mass of $M_\psi \approx 10^{-13} M_\odot$, composed of bosons with a mass of $m_\psi = 1.5 \times 10^{-14}$ eV. The red curve represents the standard neutrino flavor oscillation model S_ν (see Table I), where $n_e(r) = n_{\rm res}(E)$ [Eq. (24)]. The horizontal black lines correspond to $n_{\rm res}(E)$ for E values of 100, 11, and 4 MeV, which occur in the layer located at 0.46, 0.26, and 0.15 of the solar radius, respectively (see main text for details). In our model, active neutrinos interact with the bosons through an intermediary particle with mass m_ϕ and a coupling constant $g_{\psi\nu}$. The other curves shown use the condition $n_{\rm eff}(r) = n_{\rm res}(E)$ [Eq. (28)] for $E = 100$ MeV. These curves correspond to the models $\mathrm{R}_{a\nu}$, $\mathrm{R}_{b\nu}$, and A_i $(i = 1, 6)$ presented in Table I, with the color scheme indicated in the table.

curve. In the same figure, the horizontal lines correspond to energy values of electron neutrino equal to 100, 11, and 4 MeV, for which the resonance condition occurs for the radius of 0.46, 0.26, and 0.15 solar radius.

In general, the adiabatic and nonadiabatic nature of neutrino oscillations depends on the neutrino's energy E and the relative value of the resonance condition of $n_{\rm res}(E)$ [Eq. (24)]. For instance, if a neutrino of energy E is such that (i) $n_{\rm res}(E) \gg n_{\rm e}$, neutrinos oscillate practically as in vacuum; (ii) if $n_{\rm res}(E) \ll n_{\rm e}$, oscillations are suppressed in the presence of matter [62].

In our models, most cases correspond to adiabatic transitions, for which $P_\gamma \approx 0$. Nevertheless, it is possible to compute the contribution of the nonadiabatic component P_γ to $P_{ee}(E)$ by using Eq. (21) and the following prescription: (i) compute the value of $n_{\rm res}$ [using Eq. (24)] for each value of E (with fixed values of Δm^2_{12}, θ_{12}, and θ_{13}), (ii) calculate the scale height $h_\gamma = |n_e/(dn_e/dr)|_{r_\gamma}$ at the point r_γ, defined as $n_e(r_\gamma) = n_{\rm res}(E)$, and (iii) calculate P_γ and γ for the value of h_γ. The scale height h_γ also reads $h_\gamma = |(d \ln n_e/dr)^{-1}|_{r_\gamma}$, the reason for which will be made clear later. We also found that $h_\gamma = |(d \ln V_{cc}/dr)^{-1}|_{r_\gamma}$.

Conveniently, to properly take into account the nonadiabatic correction in Eqs. (20) and (21), we included the step function $P_{\rm H}$, defined as $P_{\rm H}(V_m - \Delta m^2_{21} \cos(2\theta_{12}))$. This function is 1 for $\Delta m^2_{21} \cos(2\theta_{12}) \leq V_m$ and is 0 otherwise (e.g., [69]).

V. SURVIVAL PROBABILITY OF ELECTRON NEUTRINOS: NEW MODEL

The survival probability of electron neutrinos [Eq. (19)] in this study can vary in comparison to the standard neutrino flavor oscillation model by two mechanisms:

(1) Variation of the mass-square differences Δm^2_{ij} and the mixing angles θ_{ij} (where $i, j = 1, 2, 3$ and $i \neq j$), related with the neutrino mass correction δm_ν resulting from the interaction of active neutrinos with the boson field ψ:
   (a) Considering only first-order perturbation, thus, the neutrino mass-squared difference reads

$$\frac{\Delta m^2_{ij}(r,t)}{\Delta m^2_{ij,o}} \approx 1 + 2\bar{\epsilon}_\psi e^{-\frac{r}{R_\psi}} \cos(m_\psi t), \qquad (25)$$

where $\Delta m^2_{ij,o} = m^2_i - m^2_j$ is the standard (undistorted) value and $\Delta m^2_{ij}(r,t)$ is the perturbed term. $\Delta m^2_{ij}(r,t)$ varies with the amplitude $\bar{\epsilon}_\psi(g_\psi, m_\psi)$ and the frequency m_ψ. In the derivation of Eq. (25), we consider that $\delta m_i/m_i \approx \delta m_\nu/m_\nu$. $\delta m_\nu/m_\nu$ is given by Eq. (8) and $\bar{\epsilon}_\psi$ by

Eq. (9). The mass-squared difference Δm^2_{ij} between neutrinos of different flavors follows the usual convection (e.g., [70]), such that $\Delta m^2_{i1} = m^2_i - m^2_1$ ($i = 2$ and 3).

(b) Similarly, the mixing angle variations is written as

$$\theta_{ij}(r,t) - \theta_{ij,o} \approx \bar{\epsilon}_\psi e^{-\frac{r}{R_\psi}} \cos(m_\psi t), \tag{26}$$

where $\theta_{ij,o}$ is the standard (undistorted) mixing angle. The indices i and j in θ_{ij} follow a convention identical to the mass-squared differences.

Equations (25) and (26) are time-dependent variations similar to the ones found by several authors, such as Krnjaic *et al.* [41] and Berlin [71], that result from the impact of ψ on neutrino flavor oscillations. However, in our case, both quantities also vary with the distance.

(2) The forward scattering of active neutrinos on the boson dark matter field ψ is taken into account by the inclusion of the new term $V_{\psi\nu_a}$ [Eq. (18)] in the matter potential diagonal matrix $\mathcal{V} = \mathrm{diag}(V_{cc} + V_{nc} + V_{\psi\nu_e}, V_{nc} + V_{\psi\nu_\mu}, V_{nc} + V_{\psi\nu_\tau})$, where $V_{cc} = \sqrt{2} G_F\, n_e(r)$ and $V_{nc} = -G_F/\sqrt{2}\, G_F n_n(r)$ correspond to the charged current (cc) that takes into account the forward scattering of ν_e with electrons and the neutral current (nc) related to the scattering of all active neutrinos with the ordinary fermions (e.g., [72]). Now, if we consider that $V_{\psi\nu_a}$ is the same for all active neutrinos, then the diagonal matrix [44] takes the standard form matter potential $\mathcal{V} = \mathrm{diag}(V_{cc}, 0, 0)$. Nevertheless, in the study we consider $g_{\nu_e} \neq g_{\nu_\mu} = g_{\nu_\tau}$, therefore, $\mathcal{V} = \mathrm{diag}(V_{\mathrm{eff}}, 0, 0)$ where $V_{\mathrm{eff}} = V_{cc} + V_{\psi\nu_e} - V_{\psi\nu_\mu}$.

In the standard model, matter potential $\mathcal{V}$ associated with the forward scattering of active neutrinos depends strongly on the properties of constitutive particles of the background medium [47,51]. Therefore, we opt to consider that these neutrinos propagate in the boson medium [37,73–76], for which the coupling constants have the following relations: $g_{\nu_e} \neq g_{\nu_\tau} = g_{\nu_\mu}$. We notice that the coupling of active neutrinos with dark matter background (including axions) have been studied in many scenarios; among other articles, see the following ones: Bœhm and Fayet [73,74], Berezhiani and Mohapatra [77], Berezhiani *et al.* [78], Mangano *et al.* [79], and van den Aarssen *et al.* [80]. Therefore, now V_{eff} reads

$$V_{\mathrm{eff}}(r) = \sqrt{2} G_F \left[n_e + \frac{g_{\psi\nu} R^2_\psi n_\psi \zeta_\phi}{m^2_\phi R^2_\psi - 4} [1 + \Psi(r)] \right], \tag{27}$$

where $g_{\psi\nu}$ is a coupling constant given by $g_{\psi\nu} = g_\psi(g_{\nu_e} - g_{\nu_\mu})/(\sqrt{2} G_F)$, and $n_e(r)$ is different from zero

TABLE I. Comparison of the parameters of various dark matter boson-neutrino models. The standard neutrino model S_ν is compared to parameter-varying models, including $R_{a\nu}$, $R_{b\nu}$, A_i, B_i, and C_i, where $\bar{\epsilon} = 10^{-3}$ is fixed, and D_i, where $\bar{\epsilon} = j \times 10^{-1}$ (with $j = 1, 2, 3, 4$) is chosen. To highlight the varying parameters across each set of models, the corresponding values of these parameters are denoted in bold. Figures 2–4 show the effective resonance density n_{eff} and the electron neutrino survival probability $\langle P_{ee}(E) \rangle$ for some models. These figures provide a comparison of the various models discussed in the article. The Sun is assumed to be inside a boson cloud with a mass of approximately $10^{-13} M_\odot$, a radius of $R_\psi = 0.783$ A.U., and a parameter of condensation $\chi_\psi = 5.7 \times 10^4$.

Model	m_ψ (eV)	m_ϕ (eV)	$g_{\psi\nu}\, G_F$	χ^2_ν	χ^2_ν per d.o.f.	Color curve
S_ν	⋯	⋯	⋯	2.73	0.55	Red
$R_{a\nu}$	1.5×10^{-14}	10^{-12}	6×10^{23}	2.76	0.69	Blue
$R_{b\nu}$	1.5×10^{-14}	10^{-12}	-5×10^{24}	2.58	0.65	Green
A_1	1.5×10^{-14}	10^{-12}	$\mathbf{3 \times 10^{24}}$	2.94	0.74	Coral
A_2	1.5×10^{-14}	10^{-12}	$\mathbf{1 \times 10^{25}}$	3.77	0.94	Gold
A_3	1.5×10^{-14}	10^{-12}	$\mathbf{5 \times 10^{25}}$	15.44	3.86	Violet
A_4	1.5×10^{-14}	10^{-12}	$\mathbf{1 \times 10^{26}}$	27.36	6.84	Lime
A_5	1.5×10^{-14}	10^{-12}	$\mathbf{-1 \times 10^{24}}$	2.68	0.67	Aqua
A_6	1.5×10^{-14}	10^{-12}	$\mathbf{-7 \times 10^{25}}$	13.23	3.31	Brown
B_1	$\mathbf{1.0 \times 10^{-14}}$	10^{-12}	6×10^{23}	2.74	0.69	⋯
B_2	$\mathbf{1.8 \times 10^{-14}}$	10^{-12}	6×10^{23}	2.80	0.70	⋯
C_1	1.5×10^{-14}	$\mathbf{10^{-20}}$	6×10^{23}	2.73	0.68	⋯
C_2	1.5×10^{-14}	$\mathbf{10^{-10}}$	1×10^{25}	2.76	0.69	⋯
C_3	1.5×10^{-14}	$\mathbf{10^{-5}}$	1×10^{25}	2.76	0.69	⋯
C_4	1.5×10^{-14}	$\mathbf{10^{5}}$	1×10^{25}	2.73	0.68	⋯
D_1	1.5×10^{-14}	10^{-12}	6×10^{23}	2.62	0.66	⋯
D_2	1.5×10^{-14}	10^{-12}	6×10^{23}	2.68	0.67	⋯
D_3	1.5×10^{-14}	10^{-12}	6×10^{23}	3.47	0.87	⋯
D_4	1.5×10^{-14}	10^{-12}	6×10^{23}	4.94	1.23	⋯

only inside the Sun (for $r \leq R_\odot$). Since g_{ν_e} and g_{ν_μ} are two free positive parameters of different magnitudes, it follows from the definition that $g_{\psi\nu}$ can be positive or negative. Accordingly, V_m in Eqs. (22) and (23) now reads $V_m = V_{\rm eff}\cos^2(\theta_{13})E$.

In the new model, we generalize the result given by Eq. (24) by introducing the effective density $n_{\rm eff}$ associated with the resonance condition as

$$n_{\rm eff}(r_\gamma) = n_{\rm res}(E) \equiv \frac{\Delta m^2_{21}}{2\sqrt{2}G_F E}\frac{\cos(2\theta_{12})}{\cos^2(\theta_{13})}, \quad (28)$$

where r_γ ($\neq h_\gamma$) is defined as the layer where the resonance condition occurs, and $V_{\rm eff} = \sqrt{2}G_F n_{\rm eff}$ [see Eq. (27)], such that $n_{\rm eff}$ reads

$$n_{\rm eff} = n_e\left[1 + \frac{n_\psi}{n_e}\zeta_\phi \frac{g_{\psi\nu}R^2_\psi}{m^2_\phi R^2_\psi - 4}[1 + \Psi(r)]\right]. \quad (29)$$

Once we assume that the second term of Eq. (29) is always positive, we therefore choose a boson such that $m_\phi \geq m_{\phi,\rm crit} = 2/R_\psi$; the conclusions found at the end of Sec. IV associated with the electronic density $n_e(r)$ remain valid for $n_{\rm eff}(r)$. For example, for $R_\phi = 0.5$ A.U. we obtain $m_{\phi,c} = 5.3 \times 10^{-27}$ GeV. Figure 2 shows $n_{\rm eff}(r)$ [Eq. (29)] of several models for the present Sun as colored curves. Table I presents the parameters of such models. Models with changed parameters are displayed in bold to aid the reader's understanding of the table. It is worth noticing that, in comparison with the classical case [Eq. (24)], neutrino oscillations in some of these new models are suppressed for higher neutrino energy values [Eq. (28)]. This is the case of models A_2 (gold curve) and A_3 (violet curve).

Similar to the standard case (model S_ν in Table I), $P_{ee}(E)$'s contribution [Eqs. (19) and (20)] coming from the jump probability P_γ, although small, is not entirely negligible in this class of models. We compute the jump probability P_γ by using expression (21) where r_γ is now determined by condition (28) and the scale height reads $h_\gamma = |(d\ln V_{\rm eff}/dr)^{-1}|_{r_\gamma}$. The contribution comes from the interaction of electron neutrinos with the boson field ϕ within the dark matter halo. Unlike in the standard case (model S_ν in Table I), the contribution is small but marginally visible for the conversion of electron neutrinos with high energy (see Fig. 1).

VI. LIGHT-DARK MATTER IMPACT ON SOLAR NEUTRINOS

The survival probability of electron neutrinos $P_{ee}(E)$ [Eq. (19)] is a time-dependent function through the time-varying boson field $\psi(t)$. Conveniently, we define the averaged survival probability of electron neutrinos as

$$\langle P_{ee}(E)\rangle = \int_0^{\tau_\psi} P_{ee}(E,\psi)\frac{dt}{\tau_\psi}, \quad (30)$$

where $\tau_\psi = 2\pi/m_\psi$ is the period of the boson field $\psi(t)$. The ability of a solar neutrino detector to measure the impact of the time-dependent field $\psi(t)$ on the averaged survival probability $\langle P_{ee}(E)\rangle$ depends on three characteristic timescales:

(1) τ_ν is the neutrino flight time, for a solar neutrino τ_ν is approximately 8.2 min.
(2) τ_{ev} is the time between two consecutive neutrino detections; for some of the forthcoming neutrinos experiments, τ_{ev} is bigger than 7 min (JUNO [81]).
(3) τ_{ex} is the total run time of the experiment, which for most detectors should be above ten years.

Since solar neutrino detectors will run for long periods and collect many events, it is reasonable to consider that τ_{ev} and τ_{ex} have small and large values, respectively. Therefore, the $\langle P_{ee}(E)\rangle$ time modulation by $\psi(t)$ depends slowly on period τ_ψ in comparison to τ_ν. Hence, from the condition that $\tau_\psi = 8.2\ \text{min} = \tau_\nu$, we obtain a critical boson mass $m_{\psi,c} = 8.3 \times 0^{-18}$ eV. This critical value defines the mass range of the two time modulation regimes that affect the survival probability function of the electron neutrinos:

(1) Low-frequency regime: $m_\psi \leq m_{\psi,c}$ (or $\tau_\psi \geq \tau_\nu$), a direct time modulation of $P_{ee}(E,\psi)$ occurs when the period of $\psi(t)$ is larger than the neutrino flight time τ_ν. In this case, a temporal variation of the neutrino signal may be observed in the $\langle P_{ee}(E)\rangle$ function. This type of physical process and the associated variation of time-dependent neutrino flux measurements were studied by Berlin [71], among others.
(2) High-frequency regime: $m_\psi \geq m_{\psi,c}$ (or $\tau_\psi \leq \tau_\nu$), the change of $P_{ee}(E,\psi)$ produced by $\psi(t)$ occurs on a timescale faster than the neutrino flight time τ_ν. The timescale of this variation is too quick to create a periodic time modulation on the neutrino flux measurements. Nevertheless, such a process leads to the existence of a distorted $\langle P_{ee}(E)\rangle$ average and a spread of the $P_{ee}(E,\psi)$, similar to an energy resolution smearing. This distorted probability average is identified by its deviation from the undistorted $\langle P_{ee}(E)\rangle$ in the standard scenario (e.g., [41]). Indeed, the net effect of averaging over time [see Eq. (30)] induces a shift in the observed values of $\langle P_{ee}(E)\rangle$ relative to its undistorted value.

The neutrino models discussed in this work are within the latter case—the high-frequency regime, once m_ψ (see Table I) is much larger than $m_{\psi,c}$ for all the models. It is worth highlighting that future neutrino detectors will obtain neutrino flux datasets that we can use to test such a range of boson masses. Examples of such class of detectors are the Deep Underground Neutrino Experiment [82] and the Jiangmen Underground Neutrino Observatory [83].

VII. TESTING ULTRALIGHT BOSONS WITH ACTIVE NEUTRINOS

To test our neutrino-boson model, we use an up-to-date standard solar model with good agreement with current neutrino fluxes and helioseismic datasets. The details about the physics of this standard solar model in which we use the AGSS09 (low-Z) solar abundances [84] are described in Lopes and Silk [36] and Capelo and Lopes [85]. The Sun's present-day structure was computed with release version 12115 of the stellar evolution code MESA (e.g., [86]). This stellar code computes one-dimensional star structures through time; thus, the code follows the evolution of the Sun from the pre-main-sequence or zero-age main sequence until the Sun's present age, 4.57 Gyr. Then, using a χ^2 calibration optimization method, Capelo and Lopes [85] obtain a present-day Sun model that better fits the observed solar values, such as the luminosity and effective temperature of the star, 3.8418×10^{33} erg s^{-1} and 5777 K, respectively. Among other quantities, the χ^2 calibration method also fits the experimental determination of the abundance stellar surface ratio: $(Z_s/X_s)_\odot = 0.0181$, where Z_s and X_s are the metal and hydrogen abundances at the star's surface [87–89].

In this nonstandard neutrino flavor oscillation model, we opt to use the parameter values corresponding to the standard neutrino oscillation model (e.g., [90]). Hence, we adopt the recent values obtained by the data analysis of the standard three-neutrino flavor oscillation model obtained by de Salas *et al.* [91]. Accordingly, for a parametrization with a normal ordering of neutrino masses, the mass-square difference and the mixing angles have the following values (see Table 3 of [91]): $\Delta m^2_{21} = 7.50^{+0.22}_{-0.20} \times 10^{-5}$ eV^2, $\sin^2\theta_{12} = 0.318 \pm 0.016$, and $\sin^2\theta_{13} = 0.02250^{+0.00055}_{-0.00078}$. Similarly, $\Delta m^2_{31} = 2.55^{+0.02}_{-0.03} \times 10^{-3}$ eV^2 and $\sin^2\theta_{23} = 0.574 \pm 0.014$. Moreover, we assume that all phases are equal to zero.

Figures 3 and 4 show the $\langle P_{ee}(E)\rangle$ [Eq. (30)] functions for different standard and nonstandard neutrino flavor oscillation models. Table I shows the parameters used to compute such models. The shape of $\langle P_{ee}(E)\rangle$ as a function of the neutrino's energy depends on the interaction of active neutrinos with the plasma background state inside the Sun and the interaction of electron neutrinos with the boson field $\psi(t)$ inside the dark matter halo. Two parameters regulate this latter interaction: the coupling constant $g_{\psi\nu}$ and the amplitude of the time variation boson field $\bar{\epsilon}$. The former defines the strength of the coupling of electron neutrinos to the boson background state; the latter fixes the amplitude of the time-varying boson field on the mass differences and mixing angles of the neutrino flavor oscillation model.

Figure 3 displays several models from Table I (including models S_ν, $R_{a\nu}$, $R_{b\nu}$, and A_i with $i = 1, 6$), where we choose positive and negative values of $g_{\psi\nu}$ ranging from $-7 \times 10^{25}\, G_F$ to $5 \times 10^{25}\, G_F$. We neglect the time variation of the boson field for now and thus set $\bar{\epsilon} = 10^{-3}$. Similar to the standard neutrino flavor oscillation model, vacuum oscillations dominate the neutrino propagation for lower-energy neutrinos ($E \leq 1$ MeV) inside the star, in the dark matter halo, and naturally in outer space. Similarly, as the neutrino energy increases ($E \geq 10$ MeV), the contribution from the active neutrinos' interaction with the solar background plasma (MSW effect) becomes equally important. In this study, for the nonstandard neutrino models, we include the interaction of electron neutrinos with the boson field $\psi(t)$ inside the dark matter halo. Overall, the neutrino oscillations and suppression are similar to the classical case, as shown in Fig. 3. However, for those neutrino-boson models with a large value of the coupling constant $g_{\psi\nu}$, the MSW effect occurs all over the boson halo, including inside and outside the Sun, and affects the propagation of all solar neutrinos. This effect is evident in model A_3 (shown by the

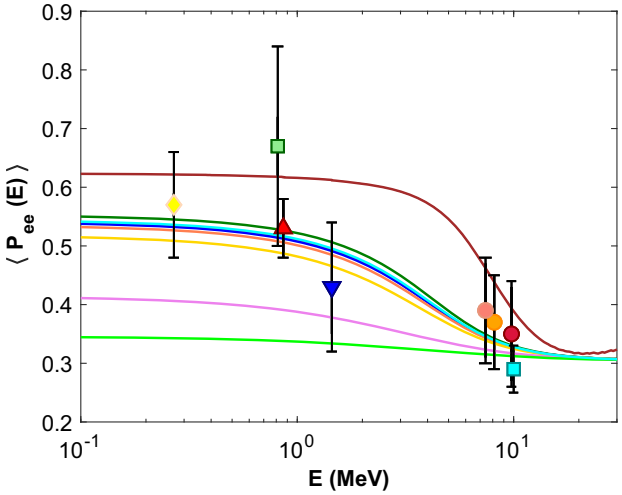

FIG. 3. Survival probability of electron neutrinos $\langle P_{ee}(E)\rangle$ in a standard three-neutrino flavor oscillation model with neutrinos, coupled to a boson dark matter field ψ with a fixed value of m_ψ (see main text). The figure shows the $\langle P_{ee}(E)\rangle$ of boson models presented in Table I with $\bar{\epsilon} = 10^{-3}$. The curves correspond to a set of models presented in Table I: S_ν (red curve, ${\chi_\nu}^2 = 2.73$), $R_{a\nu}$ (blue curve, ${\chi_\nu}^2 = 2.76$), $R_{b\nu}$ (green curve, ${\chi_\nu}^2 = 2.58$), and A_i models, for instance, A_2 (gold curve, ${\chi_\nu}^2 = 3.77$), A_3 (violet curve, ${\chi_\nu}^2 = 15.44$), and A_6 (light brown curve, ${\chi_\nu}^2 = 13.23$). The data points correspond to the survival probabilities of electron neutrinos measured by three solar neutrino detectors (SNO, Super-Kamiokande, and Borexino) and computed using a current standard solar model: (i) Borexino, pp (yellow diamond), ^{7}Be (red upward triangle), pep (blue downward triangle), and ^{8}B HER (salmon circle), ^{8}B HER-I (orange circle), and ^{8}B HER-II (magenta circle); (ii) SNO, ^{8}B (cyan square); (iii) KamLAND/SNO, ^{7}Be (green square). See Agostini *et al.* [92,93], Bellini *et al.* [94], Abe *et al.* [95,96], Aharmim *et al.* [97], Cravens *et al.* [98], and references therein, for details on the experimental data. HER, high-energy region. See the main text for more details.

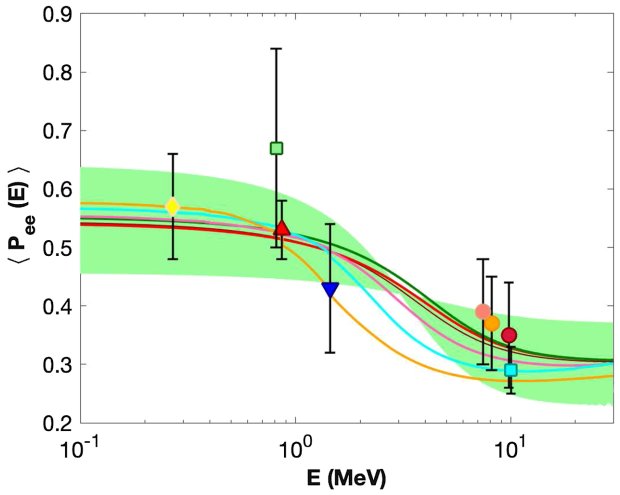

FIG. 4. The figure illustrates the averaged survival probability of ^{8}B electron neutrinos $\langle P_{ee}(E)\rangle$, resulting from the interaction of active neutrinos with the background medium. The red curve depicts the standard three-neutrino flavor oscillation model S_ν, with a χ^2_ν value of 2.73, while the blue curve represents the new neutrino-boson $R_{a\nu}$ model with $\bar{\epsilon} = 10^{-3}$ and a χ^2_ν value of 2.76. Both models are referenced in Table I. We also calculate a variant of the $R_{a\nu}$ model, denoted as D_1, where $\bar{\epsilon} = 0.1$. This version is represented by a thin brown curve and a light green band with a corresponding χ^2_ν value of 2.62. Similarly, the magenta, cyan, and orange curves represent the $\langle P_{ee}(E)\rangle$ functions for models D_2, D_3, and D_4. These are computed at $\bar{\epsilon} = 0.2$, yielding a χ^2_ν value of 2.68, at $\bar{\epsilon} = 0.3$ with a χ^2_ν of 3.47, and at $\bar{\epsilon} = 0.4$ with a χ^2_ν of 4.94, respectively. All neutrino-boson models used in this figure are detailed in Table I. The solar neutrino data are consistent with the one used in Fig. 3.

violet curve in Fig. 3). Alternatively, in the case of a negative value of $g_{\psi\nu}$, the effect is reversed, as seen in model A_6 (shown by the brown curve in Fig. 3).

In addition, to highlight the impact of this new neutrino-boson model on the $\langle P_{ee}(E)\rangle$, in Figs. 3 and 4, we show the survival probability of electron neutrinos for the standard three-neutrino flavor model (continuous red curve). Although the standard neutrino flavor oscillation model agrees with the current pp, pep, ^{7}Be, and ^{8}B measurements, only a restricted set of these nonstandard neutrino flavor models are in agreement with these solar neutrino measurements. In this work, we opt to assess the quality of these new models in fitting the data by using the following χ^2_ν statistical test:

$$\chi^2_\nu = \sum_{i=1}^{N} \left(\frac{P^{\rm obs}_{ee}(E_i) - P^{th}_{ee}(E_i)}{\sigma_{\rm obs}(E_i)} \right)^2, \qquad (31)$$

where N is the total number of data points. The above χ^2_ν combined the neutrino measurements made by several solar neutrino experiments at different energy values E_i of the survival probability function $P_{ee}(E)$. The subscript "obs" and superscript "th" indicate the observed and theoretical $\langle P_{ee}(E)\rangle$ [Eqs. (30) and (19)] values at neutrino energy E_i, and the subscript i refers to specific experimental measurement (see Fig. 3). $\sigma_{\rm obs}(E_i)$ is the error of measurement i. The data points $P^{\rm obs}_{ee}(E_i)$ are measurements obtained by solar neutrino experiments [92–98]. For convenience, we define the degree of freedom (d.o.f.) as d.o.f. $= N - k$, where N is the number of data points and k is the number of parameters in the model. In this context, the reduced chi-square value χ^2_ν, as defined in Eq. (31), is normalized by the degree of freedom to yield χ^2_ν/d.o.f., effectively providing a measure of the goodness of fit per degree of freedom. In the current study, we consider $N = 8$ data points. For the S_ν model, we have $k = 3$ parameters, leading to a degree of freedom d.o.f. $= 5$. For all other models presented in Table I, we have $k = 4$ parameters, resulting in d.o.f. $= 4$. Figures 3 and 4 illustrate a set of data points pertinent to this analysis, while Table I lists the corresponding values of χ^2_ν and χ^2/d.o.f. Interestingly, our analysis (presented in Table I) shows that the S_ν model's χ^2/d.o.f. value is lower than that of any other model considered in this study. Once that S_ν model contains fewer parameters, our findings suggest that the extra parameters employed in the other models may not be necessary for an accurate and robust representation of the current neutrino data. In line with the principle of Occam's razor, which advocates for simplicity in model selection, the S_ν model, with its optimal χ^2/d.o.f. and reduced parameter count, emerges as the most favorable model.

However, it is noteworthy that several neutrino-boson models with specific values of $g_{\psi\nu}$ and m_ψ were also found to fit the solar neutrino data, albeit not as well as the S_ν standard neutrino oscillation model. For instance, models $R_{b\nu}$ and A_5 yield χ^2_ν values that are comparable to, or even greater than, those of the S_ν model. However, these models also have larger χ^2/d.o.f. values, indicating a less optimal fit. Furthermore, several other models, including A_3, A_4, and A_6, exhibit substantially larger χ^2_ν and χ^2/d.o.f. values compared to the S_ν model. Given these findings, we can reasonably exclude these models from our consideration. Additionally, we explored the influence of m_ψ and m_ϕ on the average survival probability $\langle P_{ee}(E)\rangle$ for models B_i and C_i, as indicated in the same table. However, our findings generally suggest a minimal impact. Interestingly, we identified models such as C_1 and C_4 that exhibit a χ^2_ν identical to the standard model across a range of m_ϕ values, whether small or large.

Figure 4 presents a crucial and relevant result: the interaction of electron neutrinos with the background boson field occurs through the coupling constant $g_{\psi\nu}$ [Eq. (27)], but also depends on the amplitude $\bar{\epsilon}$ [Eq. (9)] of the boson field $\psi(t)$, which is determined by the time variation of mass difference and mixing angles [Eqs. (25) and (26)]. This figure illustrates that, compared to the standard case, the $\langle P_{ee}(E)\rangle$ of a boson-neutrino model undergoes a shift

proportional to the magnitude of $\bar{\epsilon}$. This effect is visible primarily in the 1–10 MeV energy range. Interestingly, for some of these neutrino-boson models, $\langle P_{ee}(E)\rangle$ improves the agreement with the observational data (see models D_i with $i = 1, \ldots, 4$ in Table I). Figure 4 depicts two such models, D_1 and D_2, with $\chi^2_\nu = 2.62$ and $\chi^2_\nu = 2.68$, respectively. These χ^2_ν values are smaller than the one found for the standard case ($\chi^2_\nu = 2.73$). Although these models are compatible with the current data, their χ^2/d.o.f. values are larger than that of the S_ν model. Therefore, despite their compatibility, the S_ν model remains the preferred choice.

Using $R_{a\nu}$ and $R_{b\nu}$ as reference models (see Table I), we estimate some parameter limits. Comparing models A_i $(i = 1, \ldots, 6)$ with S_ν, we find that values of the neutrino-boson coupling constant $g_{\psi\nu}$ outside the interval $-10^{24}\, G_F$ and $10^{25}\, G_F$ result in χ^2_ν values significantly higher than the $\chi^2_\nu = 2.73$ one of the standard neutrino model. Therefore, we set the following limits for the neutrino-boson coupling constant: $-10^{24}\, G_F \leq g_{\psi\nu} \leq 10^{25}\, G_F$. We also find that the boson's mass m_ψ can take any value in the interval $1.0 \times 10^{-14} - 1.8 \times 10^{-14}$ eV, which corresponds to neutrino-boson models B_1 and B_2 with $\chi^2_\nu = 4.74$ and $\chi^2_\nu = 2.80$, respectively. Finally, we conclude that the mass of the intermediate particle m_ϕ does not significantly affect the neutrino propagation.

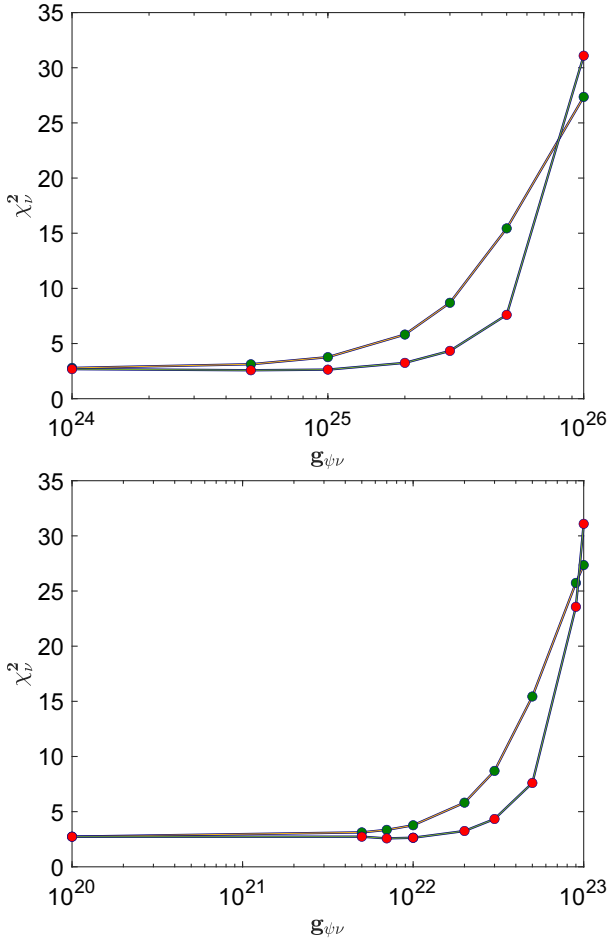

FIG. 5. The figures display the χ^2_ν test values as a function of the coupling constant $g_{\psi\nu}$ for dark matter halos with $M_\psi = 10^{-13} M_\odot$ (top) and $M_\psi = 10^{-10} M_\odot$ (bottom), respectively. In both, green circles represent positive values of g_ν in the dark matter models, while red circles represent negative values.

In Fig. 5, we plot the dependence of the parameter $g_{\psi\nu}$ on χ^2_ν for two different dark matter halo masses: $M_\psi = 10^{-10} M_\odot$ and $M_\psi = 10^{-13} M_\odot$. Although $g_{\psi\nu}$ behaves similarly in both cases, we find that the optimal range of values that agrees with the solar neutrino data is different for the two dark matter halos. Specifically, for $M_\psi = 10^{-10} M_\odot$, the agreement occurs for $g_{\psi\nu} \leq 10^{22} G_F$, whereas for $M_\psi = 10^{-13} M_\odot$, it occurs for $g_{\psi\nu} \leq 10^{25} G_F$. In both cases, we observe that the absolute value of χ^2_ν increases rapidly as $g_{\psi\nu}$ increases. We also find that negative values of $g_{\psi\nu}$ provide a better fit to the data than positive values, but for large values of $g_{\psi\nu}$, the negative solutions are overtaken by the positive ones. Our findings indicate that a very light-dark matter halo with a mass of $M_\psi = 10^{-13} M_\odot$ hosted by the Sun is consistent with the solar data. Furthermore, this agreement holds even for models with $g_{\psi\nu}$ negative values. However, despite the inclusion of additional parameters, the standard case S_ν remains the preferred choice based on the current solar data, as the improvement in the fitting procedure is not substantial. Additionally, we note that both negative solutions for $g_{\psi\nu}$ yield a small χ^2 value, albeit with a larger χ^2/d.o.f. Thus, considering the results presented in Table I, it is evident that the standard model, represented as S_ν, remains the most suitable option for fitting the current solar neutrino data.

VIII. SUMMARY AND CONCLUSION

Previous studies have shown that the gravitational field of stars, including the Sun, enhances the concentration of ultralight-dark matter particles in their vicinity, forming a stable dark matter halo. Our study explores explicitly the potential interaction between solar neutrinos and the ultralight-dark matter particles within this halo. We investigate how the survival probability of electron neutrinos is affected when active neutrinos interact with a locally enhanced, time-dependent ultralight-dark matter field, in addition to the standard interactions. This interaction is mediated by a new particle, ϕ. It causes active neutrinos to undergo flavor neutrino oscillations and MSW effects, as determined by the time-dependent mass term $\delta m_\nu / m_\nu$, the neutrino mixing angles, and a new term in the matter potential diagonal matrix $\mathcal{V}$, which defines the neutrino's interaction with the boson field $V_{\nu\phi}$.

Our investigation reveals that the impact of solar bosonic dark matter on solar neutrinos can be categorized into two

classes: (i) The effect is significant to the extent that such models can be conclusively rejected based on current data. (ii) The impact is minimal, and the additional freedom does not improve the agreement between the models and the data.

Here, we showcase the robustness of the current agreement between the standard flavor oscillation model and the data, making it very difficult to challenge. Even with the incorporation of ultralight bosons, substantial couplings, and the inclusion of a mediator, the standard model maintains its strong compatibility with the data. This finding aligns with previous research by [42], which also revealed a similar outcome regarding the average local dark matter density. Our study further confirms that this challenge persists even when considering a highly dense halo confined within the Sun. However, it is worth noting that as more data become available, it remains possible to disregard these models or discover potential improvements in the future. The validation of such a class of models will be tested by the next generation of neutrino detectors, including hybrid optical neutrino detectors, such as Theia [99], Jinping [100] and Yemilab [101], or by liquid scintillator experiments like JUNO [83,102] and SNO+ [103] and water Cherenkov experiments such as Hyper-Kamiokande [104] and DUNE [105].

ACKNOWLEDGMENTS

I. L. thanks Fundação para a Ciência e Tecnologia (FCT), Portugal, for the financial support to the Center for Astrophysics and Gravitation (CENTRA/IST/ULisboa) through the Grant Project No. UIDB/00099/2020 and Grant No. PTDC/FIS-AST/28920/2017.

[1] F. Zwicky, Helv. Phys. Acta **6**, 110 (1933), https://ui.adsabs.harvard.edu/abs/1933AcHPh...6..110Z.
[2] M. Battaglieri, A. Belloni, A. Chou, P. Cushman, B. Echenard, R. Essig, J. Estrada, J. L. Feng, B. Flaugher, P. J. Fox *et al.*, arXiv:1707.04591.
[3] J. L. Feng, Annu. Rev. Astron. Astrophys. **48**, 495 (2010).
[4] H. Baer, K.-Y. Choi, J. E. Kim, and L. Roszkowski, Phys. Rep. **555**, 1 (2015).
[5] P. Agrawal, M. Bauer, J. Beacham, A. Berlin, A. Boyarsky, S. Cebrian, X. Cid-Vidal, D. d'Enterria, A. De Roeck, M. Drewes *et al.*, Eur. Phys. J. C **81**, 1015 (2021).
[6] P. W. Graham, I. G. Irastorza, S. K. Lamoreaux, A. Lindner, and K. A. van Bibber, Annu. Rev. Nucl. Part. Sci. **65**, 485 (2015).
[7] L. Ackerman, M. R. Buckley, S. M. Carroll, and M. Kamionkowski, Phys. Rev. D **79**, 023519 (2009).
[8] L. Di Luzio, M. Giannotti, E. Nardi, and L. Visinelli, Phys. Rep. **870**, 1 (2020).
[9] D. J. E. Marsh, Phys. Rep. **643**, 1 (2016).
[10] S. J. Asztalos, G. Carosi, C. Hagmann, D. Kinion, K. van Bibber, M. Hotz, L. J. Rosenberg, G. Rybka, J. Hoskins, J. Hwang *et al.*, Phys. Rev. Lett. **104**, 041301 (2010).
[11] D. Budker, P. W. Graham, M. Ledbetter, S. Rajendran, and A. O. Sushkov, Phys. Rev. X **4**, 021030 (2014).
[12] Y. V. Stadnik and V. V. Flambaum, Phys. Rev. D **89**, 043522 (2014).
[13] G. D. Orebi Gann, K. Zuber, D. Bemmerer, and A. Serenelli, Annu. Rev. Nucl. Part. Sci. **71**, 491 (2021).
[14] J. A. Dror, H. Murayama, and N. L. Rodd, Phys. Rev. D **103**, 115004 (2021).
[15] J. Billard, M. Boulay, S. Cebrián, L. Covi, G. Fiorillo, A. Green, J. Kopp, B. Majorovits, K. Palladino, F. Petricca *et al.*, Rep. Prog. Phys. **85**, 056201 (2022).
[16] L. Hui, J. P. Ostriker, S. Tremaine, and E. Witten, Phys. Rev. D **95**, 043541 (2017).
[17] J. C. Niemeyer, Prog. Part. Nucl. Phys. **113**, 103787 (2020).
[18] R. Catena and P. Ullio, J. Cosmol. Astropart. Phys. 08 (2010) 004.
[19] N. Aghanim, Y. Akrami, M. Ashdown, J. Aumont, C. Baccigalupi, M. Ballardini, A. J. Banday, R. B. Barreiro, N. Bartolo *et al.* (Planck Collaboration), Astron. Astrophys. **641**, A6 (2020).
[20] I. Lopes and S. Turck-Chièze, Astrophys. J. **765**, 14 (2013).
[21] L. F. Abbott and P. Sikivie, Phys. Lett. **120B**, 133 (1983).
[22] A. Khmelnitsky and V. Rubakov, J. Cosmol. Astropart. Phys. 02 (2014) 019.
[23] D. Blas, D. L. Nacir, and S. Sibiryakov, Phys. Rev. Lett. **118**, 261102 (2017).
[24] M. Colpi, S. L. Shapiro, and I. Wasserman, Phys. Rev. Lett. **57**, 2485 (1986).
[25] S. L. Liebling and C. Palenzuela, Living Rev. Relativity **15**, 6 (2012).
[26] D. J. Kaup, Phys. Rev. **172**, 1331 (1968).
[27] R. Ruffini and S. Bonazzola, Phys. Rev. **187**, 1767 (1969).
[28] J. A. Wheeler, Phys. Rev. **97**, 511 (1955).
[29] E. Braaten and H. Zhang, Rev. Mod. Phys. **91**, 041002 (2019).
[30] M. H. Namjoo, A. H. Guth, and D. I. Kaiser, Phys. Rev. D **98**, 016011 (2018).
[31] P.-H. Chavanis, Phys. Rev. D **84**, 043531 (2011).
[32] J. Eby, M. Leembruggen, L. Street, P. Suranyi, and L. C. R. Wijewardhana, Phys. Rev. D **98**, 123013 (2018).
[33] C. G. Böhmer and T. Harko, J. Cosmol. Astropart. Phys. 06 (2007) 025.
[34] A. Banerjee, D. Budker, J. Eby, V. V. Flambaum, H. Kim, O. Matsedonskyi, and G. Perez, J. High Energy Phys. 09 (2020) 004.
[35] A. Banerjee, D. Budker, J. Eby, H. Kim, and G. Perez, Commun. Phys. **3**, 1 (2020).

[36] I. Lopes and J. Silk, Mon. Not. R. Astron. Soc. **435**, 2109 (2013).
[37] O. G. Miranda, C. A. Moura, and A. Parada, Phys. Lett. B **744**, 55 (2015).
[38] C. A. Argüelles, A. J. Aurisano, B. Batell, J. Berger, M. Bishai, T. Boschi, N. Byrnes, A. Chatterjee, A. Chodos, T. Coan *et al.*, Rep. Prog. Phys. **83**, 124201 (2020).
[39] M. C. Gonzalez-Garcia and M. Maltoni, Phys. Rep. **460**, 1 (2008).
[40] A. Y. Smirnov and X.-J. Xu, J. High Energy Phys. 12 (2019) 046.
[41] G. Krnjaic, P. A. N. Machado, and L. Necib, Phys. Rev. D **97**, 075017 (2018).
[42] I. Lopes, Astrophys. J. **905**, 22 (2020).
[43] A. Y. Smirnov and V. B. Valera, J. High Energy Phys. 02 (2021) 177.
[44] T. K. Kuo and J. Pantaleone, Rev. Mod. Phys. **61**, 937 (1989).
[45] L. Wolfenstein, Phys. Rev. D **17**, 2369 (1978).
[46] S. P. Mikheyev and A. Y. Smirnov, Yad. Fiz. **42**, 1441 (1985).
[47] F. J. Botella, C. S. Lim, and W. J. Marciano, Phys. Rev. D **35**, 896 (1987).
[48] J. C. D'olivo, J. F. Nieves, and M. Torres, Phys. Rev. D **46**, 1172 (1992).
[49] C. Lunardini and A. Y. Smirnov, Nucl. Phys. **B583**, 260 (2000).
[50] T. Konstandin and T. Ohlsson, Phys. Lett. B **634**, 267 (2006).
[51] D. Nötzold and G. Raffelt, Nucl. Phys. **B307**, 924 (1988).
[52] W. C. Haxton, Phys. Rev. Lett. **57**, 1271 (1986).
[53] S. J. Parke, Phys. Rev. Lett. **57**, 1275 (1986).
[54] I. Lopes, Phys. Rev. D **88**, 045006 (2013).
[55] W. C. Haxton, R. G. Hamish Robertson, and A. M. Serenelli, Annu. Rev. Astron. Astrophys. **51**, 21 (2013).
[56] J. F. Beacom, S. Chen, J. Cheng, S. N. Doustimotlagh, Y. Gao, G. Gong, H. Gong, L. Guo, R. Han, H.-J. He *et al.*, Chin. Phys. C **41**, 023002 (2017).
[57] M. C. Gonzalez-Garcia and Y. Nir, Rev. Mod. Phys. **75**, 345 (2003).
[58] G. Fantini, A. Gallo Rosso, F. Vissani, and V. Zema, Adv. Ser. Dir. High Energy Phys. **28**, 37 (2018).
[59] J. N. Bahcall and C. Peña-Garay, New J. Phys. **6**, 63 (2004).
[60] S. Kumaran, L. Ludhova, Ö. Penek, and G. Settanta, Universe **7**, 231 (2021).
[61] M. Tanabashi, K. Hagiwara, K. Hikasa, K. Nakamura, Y. Sumino, F. Takahashi, J. Tanaka, K. Agashe, G. Aielli, C. Amsler *et al.*, Phys. Rev. D **98**, 030001 (2018).
[62] C. Patrignani, K. Agashe, G. Aielli, C. Amsler, M. Antonelli, D. M. Asner, H. Baer, S. Banerjee, R. M. Barnett *et al.* (Particle Data Group), Chin. Phys. C **40**, 100001 (2016).
[63] T. K. Kuo and J. Pantaleone, Phys. Rev. D **39**, 1930 (1989).
[64] M. Bruggen, W. C. Haxton, and Y. Z. Qian, Phys. Rev. D **51**, 4028 (1995).
[65] A. de Gouvêa, Nucl. Instrum. Methods Phys. Res., Sect. A **503**, 4 (2003).
[66] A. d. Gouvêa, A. Friedland, and H. Murayama, Phys. Lett. B **490**, 125 (2000).
[67] A. Gando, Y. Gando, K. Ichimura, H. Ikeda, K. Inoue, Y. Kibe, Y. Kishimoto, M. Koga, Y. Minekawa, T. Mitsui *et al.*, Phys. Rev. D **83**, 052002 (2011).
[68] P. C. de Holanda, W. Liao, and A. Y. Smirnov, Nucl. Phys. **B702**, 307 (2004).
[69] H. Casini, J. C. D'olivo, and R. Montemayor, Phys. Rev. D **61**, 105004 (2000).
[70] I. Lopes, Phys. Rev. D **95**, 015023 (2017).
[71] A. Berlin, Phys. Rev. Lett. **117**, 231801 (2016).
[72] Z.-z. Xing, Phys. Rep. **854**, 1 (2020).
[73] C. Bœhm and P. Fayet, Nucl. Phys. **B683**, 219 (2004).
[74] P. Fayet, Phys. Rev. D **75**, 115017 (2007).
[75] A. Ioannisian and S. Pokorski, Phys. Lett. B **782**, 641 (2018).
[76] K.-Y. Choi, E. J. Chun, and J. Kim, Phys. Dark Universe **30**, 100606 (2020).
[77] Z. G. Berezhiani and R. N. Mohapatra, Phys. Rev. D **52**, 6607 (1995).
[78] Z. G. Berezhiani, A. D. Dolgov, and R. N. Mohapatra, Phys. Lett. B **375**, 26 (1996).
[79] G. Mangano, A. Melchiorri, P. Serra, A. Cooray, and M. Kamionkowski, Phys. Rev. D **74**, 043517 (2006).
[80] L. G. van den Aarssen, T. Bringmann, and C. Pfrommer, Phys. Rev. Lett. **109**, 231301 (2012).
[81] T. Adam, F. An, G. An, Q. An, N. Anfimov, V. Antonelli, G. Baccolo, M. Baldoncini, E. Baussan, M. Bellato *et al.*, arXiv:1508.07166.
[82] R. Acciarri, M. A. Acero, M. Adamowski, C. Adams, P. Adamson, S. Adhikari, Z. Ahmad, C. H. Albright, T. Alion *et al.* (DUNE Collaboration), arXiv:1512.06148.
[83] F. An, G. An, Q. An, V. Antonelli, E. Baussan, J. Beacom, L. Bezrukov, S. Blyth, R. Brugnera, M. Buizza Avanzini *et al.*, J. Phys. G Nucl. Phys. **43**, 030401 (2016).
[84] M. Asplund, N. Grevesse, A. J. Sauval, and P. Scott, Annu. Rev. Astron. Astrophys. **47**, 481 (2009).
[85] D. Capelo and I. Lopes, Mon. Not. R. Astron. Soc. **498**, 1992 (2020).
[86] B. Paxton, R. Smolec, J. Schwab, A. Gautschy, L. Bildsten, M. Cantiello, A. Dotter, R. Farmer, J. A. Goldberg, A. S. Jermyn *et al.*, Astrophys. J. Suppl. Ser. **243**, 10 (2019).
[87] S. Turck-Chieze and I. Lopes, Astrophys. J. **408**, 347 (1993).
[88] J. N. Bahcall, M. H. Pinsonneault, and G. J. Wasserburg, Rev. Mod. Phys. **67**, 781 (1995).
[89] J. N. Bahcall, A. M. Serenelli, and S. Basu, Astrophys. J. Suppl. Ser. **165**, 400 (2006).
[90] M. C. Gonzalez-Garcia, M. Maltoni, and T. Schwetz, Nucl. Phys. **B908**, 199 (2016).
[91] P. F. de Salas, D. V. Forero, S. Gariazzo, P. Martínez-Miravé, O. Mena, C. A. Ternes, M. Tórtola, and J. W. F. Valle, J. High Energy Phys. 02 (2021) 071.
[92] M. Agostini, K. Altenmüller, S. Appel, V. Atroshchenko, Z. Bagdasarian, D. Basilico, G. Bellini, J. Benziger, D. Bick *et al.* (Borexino Collaboration), Nature (London) **562**, 505 (2018).
[93] M. Agostini, K. Altenmüller, S. Appel, V. Atroshchenko, Z. Bagdasarian, D. Basilico, G. Bellini, J. Benziger, G. Bonfini, D. Bravo *et al.*, Phys. Rev. D **100**, 082004 (2019).
[94] G. Bellini, J. Benziger, S. Bonetti, M. Buizza Avanzini, B. Caccianiga, L. Cadonati, F. Calaprice, C. Carraro,

A. Chavarria, A. Chepurnov *et al.*, Phys. Rev. D **82**, 033006 (2010).
[95] S. Abe, K. Furuno, A. Gando, Y. Gando, K. Ichimura, H. Ikeda, K. Inoue, Y. Kibe, W. Kimura, Y. Kishimoto *et al.*, Phys. Rev. C **84**, 035804 (2011).
[96] K. Abe, Y. Haga, Y. Hayato, M. Ikeda, K. Iyogi, J. Kameda, Y. Kishimoto, L. Marti, M. Miura, S. Moriyama *et al.*, Phys. Rev. D **94**, 052010 (2016).
[97] B. Aharmim, S. N. Ahmed, A. E. Anthony, N. Barros, E. W. Beier, A. Bellerive, B. Beltran, M. Bergevin, S. D. Biller, K. Boudjemline *et al.*, Phys. Rev. C **88**, 025501 (2013).
[98] J. P. Cravens, K. Abe, T. Iida, K. Ishihara, J. Kameda, Y. Koshio, A. Minamino, C. Mitsuda, M. Miura, S. Moriyama *et al.*, Phys. Rev. D **78**, 032002 (2008).
[99] M. Askins, Z. Bagdasarian, N. Barros, E. W. Beier, E. Blucher, R. Bonventre, E. Bourret, E. J. Callaghan, J. Caravaca, M. Diwan *et al.*, Eur. Phys. J. C **80**, 416 (2020).
[100] J.-P. Cheng, K.-J. Kang, J.-M. Li, J. Li, Y.-J. Li, Q. Yue, Z. Zeng, Y.-H. Chen, S.-Y. Wu, X.-D. Ji *et al.*, Annu. Rev. Nucl. Part. Sci. **67**, 231 (2017).
[101] S.-H. Seo, arXiv:1903.05368.
[102] JUNO Collaboration, Prog. Part. Nucl. Phys. **123**, 103927 (2022).
[103] M. R. Anderson, S. Andringa, L. Anselmo, E. Arushanova, S. Asahi, M. Askins, D. J. Auty, A. R. Back *et al.* (SNO + Collaboration), J. Instrum. **16**, P05009 (2021).
[104] K. Abe, K. Abe, H. Aihara, A. Aimi, R. Akutsu, C. Andreopoulos, I. Anghel, L. H. V. Anthony *et al.* (Hyper-Kamiokande Proto-Collaboration), arXiv:1805.04163.
[105] R. Acciarri, M. A. Acero, M. Adamowski, C. Adams, P. Adamson, S. Adhikari, Z. Ahmad, C. H. Albright, T. Alion, E. Amador *et al.*, arXiv:1601.02984.